Journal of Physics: Condensed Matter

PAPER

# Ir 5*d*-band derived superconductivity in $LaIr_3$

To cite this article: A Bhattacharyya *et al* 2020 *J. Phys.: Condens. Matter* **32** 065602

IOP Publishing Journal of Physics: Condensed Matter
J. Phys.: Condens. Matter **32** (2020) 065602 (7pp) https://doi.org/10.1088/1361-648X/ab4389

# Ir 5*d*-band derived superconductivity in $LaIr_3$

**A Bhattacharyya[1], D T Adroja[2,3], P K Biswas[2], Y J Sato[4,5], M R Lees[6], D Aoki[5] and A D Hillier[2]**

[1] Department of Physics, Ramakrishna Mission Vivekananda Educational and Research Institute, Belur Math, Howrah 711202, West Bengal, India
[2] ISIS Facility, Rutherford Appleton Laboratory, Chilton, Didcot Oxon, OX11 0QX, United Kingdom
[3] Highly Correlated Matter Research Group, Physics Department, University of Johannesburg, PO Box 524, Auckland Park 2006, South Africa
[4] Graduate School of Engineering, Tohoku University, Sendai 980-8577, Japan
[5] Institute for Materials Research, Tohoku University, Oarai, Ibaraki 311-1313, Japan
[6] Department of Physics, University of Warwick, Coventry CV4 7AL, United Kingdom

E-mail: amitava.bhattacharyya@rkmvu.ac.in and devashibhai.adroja@stfc.ac.uk

Received 2 July 2019, revised 6 September 2019
Accepted for publication 11 September 2019
Published 7 November 2019

**Abstract**

The superconducting properties of rhombohedral $LaIr_3$ were examined using susceptibility, resistivity, heat capacity, and zero-field (ZF) and transverse-field (TF) muon spin relaxation and rotation ($\mu$SR) measurements. The susceptibility and resistivity measurements confirm a superconducting transition below $T_C = 2.5(1)$ K. Two successive transitions are observed in the heat capacity data, one at $T_C = 2.5$ K and a second at 1.2 K below $T_C$. The heat capacity jump is $\Delta C/\gamma T_C \sim 1.0$, which is lower than 1.43 expected for Bardeen–Cooper–Schrieffer (BCS) weak-coupling limit. TF-$\mu$SR measurements reveal a fully gapped *s*-wave superconductivity with $2\Delta(0)/k_BT_C = 3.31(8)$, which is small compared to the BCS value of 3.56, suggesting weak-coupling superconductivity. The magnetic penetration depth, $\lambda_L(0)$, estimated from TF-$\mu$SR gives $\lambda_L(0) = 386(3)$ nm, a superconducting carrier density $n_s = 2.9(1) \times 10^{27}$ carriers $m^{-3}$ and a carrier effective-mass enhancement factor $m^* = 1.53(1)m_e$. ZF-$\mu$SR data show no evidence for any spontaneous magnetic fields below $T_C$, which demonstrates that time-reversal symmetry is preserved in the superconducting state of $LaIr_3$.

Keywords: superconducting gap structure, d-band superconductivity, muon spin spectroscopy

(Some figures may appear in colour only in the online journal)

## 1. Introduction

The search for unconventional superconductivity in 5*d* transition metal-based compounds is one of the most fascinating and significant problems in condensed matter physics [1–4]. Due to the presence of strong spin–orbit (SO) coupling effects, the 5*d* transition metal compounds have been extensively studied to investigate the correlation between strong SO coupling and unconventional superconductivity [5, 6]. Similar energy scales for the comparatively weak electronic correlations (0.5–3 eV), crystal-field effects (1–5 eV) and strong relativistic SO coupling effects (0.1–1 eV) provide an opportunity to investigate the science emerging from competing orbital, spin, charge, and lattice degrees of freedom [7, 8]. For example, pressure-induced superconductivity in 1T-$TaS_2$ [9], in noncentrosymmetric $CePt_3Si$ [10], and in the geometrically frustrated pyrochlore oxides $Cd_2Re_2O_7$ [11] and $KOs_2O_6$ [12]. In iridium-containing compounds, superconductivity has been reported in materials such as $IrSe_2$, $Cu_{1-x}Zn_xIr_2S_4$, $CeIrSi_3$, ScIrP, LaIrP and LaIrAs, and in the ternary $ThCr_2Si_2$-type compounds $BaIr_2P_2$ and $SrIr_2As_2$ [13–18]. In the case of the rare-earth Ir based superconductors, their electronic characteristics are anticipated to arise principally from the rare-earths, rather than the Ir. Nevertheless, there are a few materials such as $CaIr_2$ [19], IrGe [20], and $Mg_{10}Ir_{19}B_{16}$ [21], where the superconductivity emerges from the Ir 5*d* states. Now, with the discovery of $LaIr_3$, there is a simple La–Ir superconductor with strong SO-coupling whose characteristics are controlled by the Ir 5*d* bands at the Fermi surface.

Recently, Haldolaarachchige *et al* [22] reported that $LaIr_3$ shows superconductivity with a $T_C$ between 2.45 and 3.3 K and $H_{c2}(0) = 38.4$ kOe, where the Fermi surface is governed by the Ir 5*d* bands that are heavily influenced by SO coupling and there is no strong contribution from the La-orbitals near $E_F$. $LaIr_3$ is, therefore, one of the few superconductors where 5*d* bands play a principal role in the appearance of superconductivity. Furthermore, a three-dimensional metallic character is seen from the band structure calculations; many bands with large dispersion cross $E_F$ [22]. $LaIr_3$ forms with a rhombohedral crystal structure with the space group $R\bar{3}m$ (166, $D^5_{3d}$). There are two crystallographically inequivalent La sites and three Ir sites [22]. To examine the role of the lanthanide elements and the SO coupling effects arising from the Ir 5*d* bands, the study of other rhombohedral $RIr_3$ materials (*R* is a lanthanide with 4*f* electrons) [23, 24] will be important. In particular, compounds with partly filled 4*f* orbitals, such as Ce and Pr, may exhibit magnetism and possibly superconductivity. Sato *et al* [24] reported that $CeIr_3$ is a type-II superconductor with a $T_C = 3.4$ K, which is the second highest $T_C$ amongst the Ce-based compounds. The small value of the Sommerfield coefficient, 23 mJ $K^{-2}$ $mol^{-1}$, indicates that $CeIr_3$ is a weakly correlated electron system [24]. The band structure and Fermi surface of $LaIr_3$ with and without SO coupling differ significantly [22], which indicates that SO coupling is expected to have a strong effect on the superconducting properties of $LaIr_3$. The role of SO coupling is further confirmed by the evidence that $T_C$ is lower in the isostructural $LaRh_3$ compound [25], where the SO coupling is negligible. $LaIr_3$ is thus a rare example of a lanthanide superconductor with strong SO coupling arising from the Ir-5*d* electrons.

In this paper, we examine the superconducting features of $LaIr_3$ using susceptibility, resistivity, heat capacity, and zero-field (ZF) and transverse-field (TF) muon spin relaxation and rotation ($\mu$SR) measurements. The TF-$\mu$SR measurements suggest an isotropic *s*-wave model can describe the superconducting ground state of $LaIr_3$. The ZF-$\mu$SR data show no evidence for internal magnetic fields below $T_C$, implying time-reversal symmetry is preserved for $LaIr_3$.

## 2. Experimental details

Polycrystalline samples of $LaIr_3$ were prepared by arc melting the constituent elements using a tri-arc furnace. The crystal structure was determined by powder x-ray diffraction utilizing a Panalytical X-Pert Pro diffractometer. Energy dispersive x-ray spectroscopy (EDS) in an FEI XL30 FEG-SEM system was used to investigate the stoichiometry (ratio of La:Ir) of the sample, and revealed an average chemical composition of $LaIr_{3.1}$, a composition with a slight excess of Ir. Zero-field-cooled (ZFC) and field-cooled (FC) DC magnetic susceptibility measurements were made using a Quantum Design (QD) Magnetic Property Measurement System (MPMS), superconducting quantum interference device magnetometer. Heat capacity was measured as a function of temperature *T* down to 350 mK in applied magnetic fields *H* of up to 60 kOe using a two-$\tau$ relaxation technique in a QD Physical Property Measurement System (PPMS) with a He-3 insert. The measurements were carried out on a solid piece of a sample taken from the arc-melted button. Resistivity measurements as a function of temperature at fixed applied field and as a function of applied field at fixed temperature were made in a QD PPMS. The sample was cut into an approximately rectangular bar. Silver wires were fixed to the sample in a four-point geometry using DuPont 4929N silver paste. Measurements at higher temperature (1.8–3 K) in fields up to 6 kOe were made using an AC technique with an excitation current of 1 mA at a frequency of 113 Hz. Measurements at lower temperature (0.5–2 K) in fields up to 12 kOe were made with a He-3 insert using a pseudo-AC method, with a 400 mA DC current passed through the sample in both directions. The upper critical field was taken to be at the midpoint of the transition from the normal into the superconducting state.

$\mu$SR measurements were performed using the MuSR spectrometer at the ISIS Neutron and Muon Source, Rutherford Appleton Laboratory, United Kingdom. In the ZF mode, 64 detectors were placed in a longitudinal configuration and in the TF mode, the spectrometer was rotated by 90°. The arc-melted button of $LaIr_3$ was ground to a fine powder and mounted on a high purity (99.995%) silver plate using GE varnish. The sample was then cooled down to 100 mK using a dilution refrigerator. During the ZF measurements, the magnetic field at the sample position was held at less than 10 mOe by an active compensation system. The muon beam is deposited in the sample and the muons decay, with the emitted positrons counted in detectors placed either forward or backward of the initial muon spin direction. The time dependence of the asymmetry spectra were determined using $G_z(t) = [N_F(t) - \alpha N_B(t)]/[N_F(t) + \alpha N_B(t)]$, where $N_B(t)$ and $N_F(t)$ are the numbers of positron counts and the constant $\alpha$ can be calculated from a calibration measurement made in a TF of 20 Oe. The ZF and TF-$\mu$SR data were analyzed using the WiMDA software [26].

## 3. Results and discussion

### 3.1. Crystal structures and magnetization

Powder x-ray diffraction data confirmed the rhombohedral structure of the $LaIr_3$ sample with the space group 166 ($R\bar{3}m$) [22]. Figure 1(a) shows the crystal structure of $LaIr_3$. The unit cell of $LaIr_3$ contains two distinct La sites (La1 and La2) and three Ir sites (Ir1, Ir2, and Ir3). The superconductivity in $LaIr_3$ was confirmed by the ZFC and FC susceptibility $\chi(T)$ data, as shown in figure 1(b). The low-field $\chi(T)$ data demonstrate a strong diamagnetic signal resulting from the Meissner effect below $T_C = 2.5$ K. The magnetization $M(H)$ curve at 2 K shown in the inset of figure 1(b) suggests

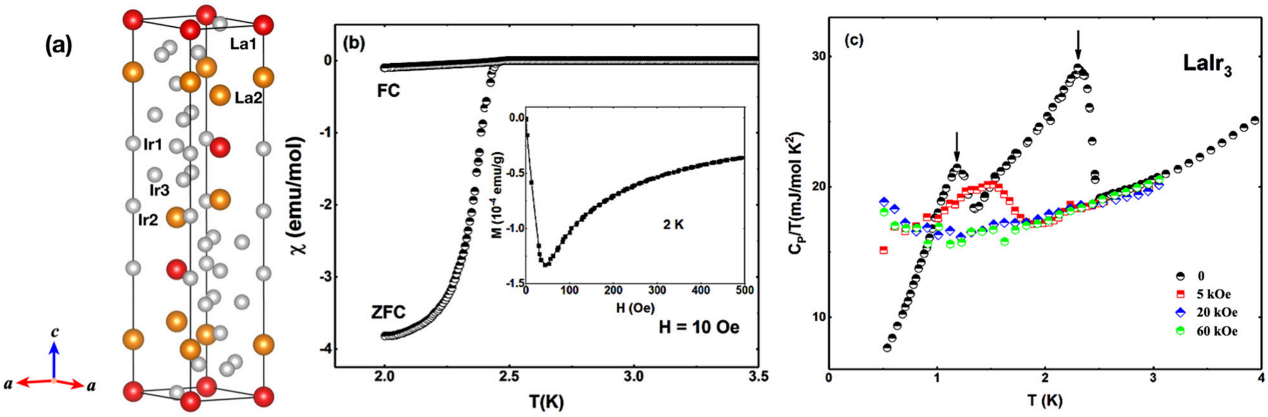


**Figure 1.** (a) Crystal structure of rhombohedral $LaIr_3$. The red spheres represent La1 atoms, yellow spheres are La2 atoms, and the small grey spheres represent the Ir atoms (Ir1, Ir2, and Ir3). (b) Susceptibility as a function of temperature of $LaIr_3$ with $H = 10$ Oe collected using ZFC and FC protocols. Inset of (b) shows the isothermal field dependence of the magnetization at 2 K. (c) $C_P/T$ versus $T$ in different applied magnetic fields.

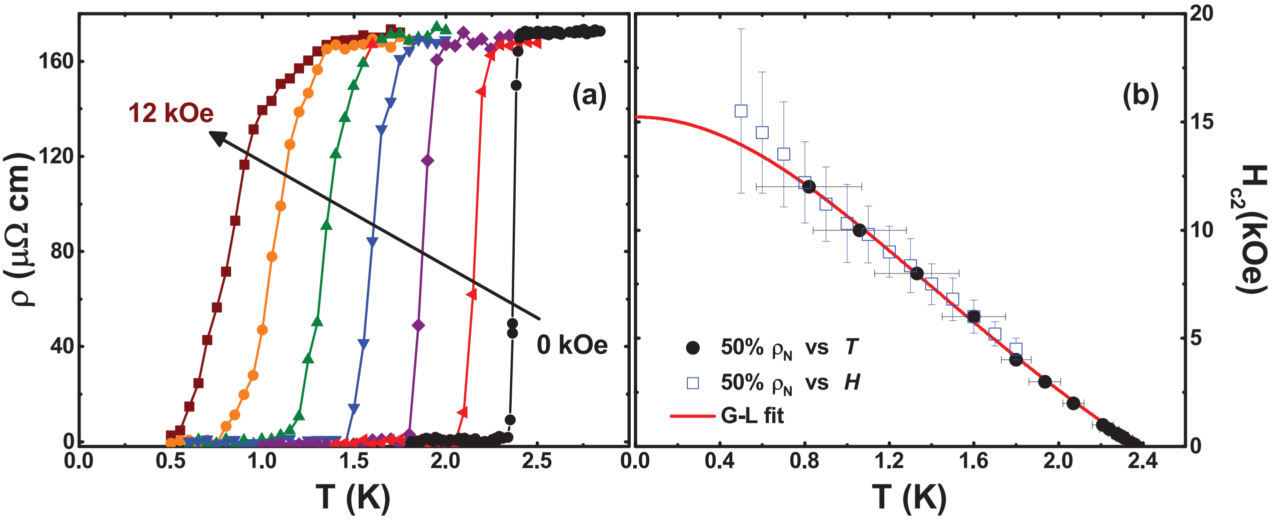


**Figure 2.** (a) Resistivity versus temperature in applied magnetic fields of 0–12 kOe in 2 kOe increments. (b) Upper critical field as a function of temperature, determined from $\rho$ versus $T$ measurements. The solid red line shows a fit using the Ginzburg–Landau (GL) model.

type-II superconductivity. The lower critical field is found to be around 35 Oe at 2 K.

### 3.2. Resistivity

The temperature dependence of the electrical resistivity for $LaIr_3$ between 50 mK and 3.0 K in various applied magnetic fields is presented in figure 2(a). In zero field, the resistivity of $LaIr_3$ undergoes a superconducting transition at $T_C = 2.4$ K. It is to be noted that the resistivity in the normal state just above the transition temperature of our sample is higher (by a factor of 5) than the value reported by Haldolaarachchige *et al* [22]. This could be due to micro-cracks in our sample. As expected, the superconducting transition becomes broader and the $T_C$ shifts to lower temperature as the applied magnetic field is increased. The resistivity data were used to extract the upper critical field $H_{c2}$. The $H_{c2}(T)$ data at higher temperature and lower field can be fit using a standard GL expression, $H_{c2}(T) = H_{c2}(0)\ [(1-t^2)]/[(1+t^2)]$, where $t = T/T_C$ giving $H_{c2}(0) = 15.2(1)$ kOe. This is lower than the value reported by Haldolaarachchige *et al* [22]. Near $T_C$, $\frac{dH_{c2}}{dT} = -6.6$ kOe $K^{-1}$, and using the Werthamer–Helfand–Hohenberg expression $H_{c2}(0) = -0.693\ T_C\ \frac{dH_{c2}}{dT}\Big|_{T=T_C}$ gave an upper critical field, $H_{c2}(0) = 10.9(1)$ kOe, which is also lower than the value obtained in [22]. Both the values of $H_{c2}(0)$ are also smaller than the weak-coupling Pauli-paramagnetic limit $H_P = 18.3T_C = 43.4$ kOe for $LaIr_3$.

### 3.3. Heat capacity

Figure 1(c) shows $C_P(T)/T$ in different applied magnetic fields. At 2.5 K, a clear anomaly is detected in $C_P(T)/T$ (in ZF) implying bulk superconductivity, in agreement with the $\chi(T)$ data. In contrast to [22], the $LaIr_3$ sample studied here exhibits a consistent transition temperature from various different measurements, indicating that 2.4–2.5 K is the bulk $T_C$ of this material. A second transition is observed in the heat capacity at 1.2 K, which is reminiscent of the second peak seen in the heat capacity of superconducting $UPt_3$ [27]. Our

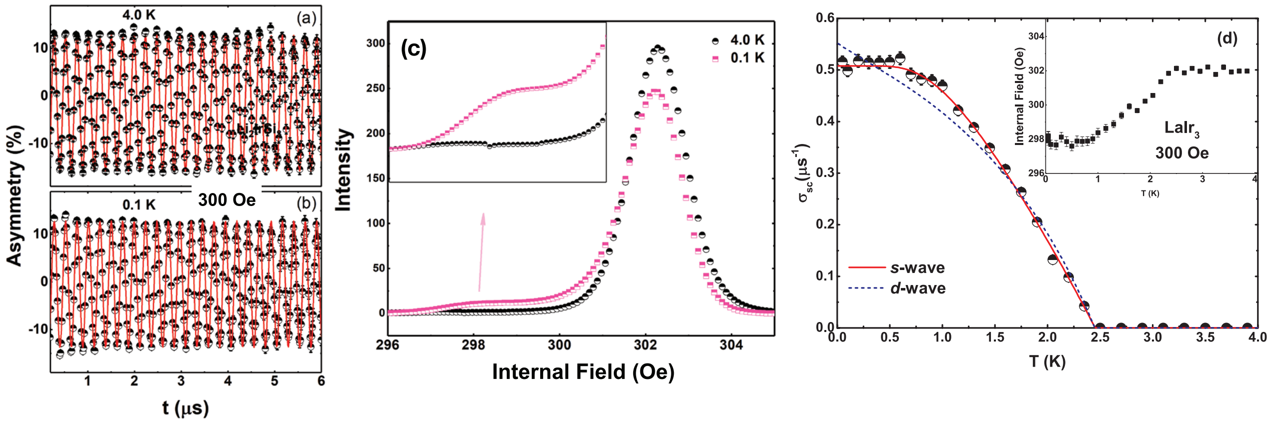


**Figure 3.** TF-$\mu$SR spin precession signals of $LaIr_3$ taken at $H = 300$ Oe. Time dependence asymmetry spectra (a) at 4.0 K, above $T_C$ and (b) at 0.1 K, below $T_C$. The solid red lines indicate the fits to the data using equation (1). (c) Maximum entropy spectra (above and below $T_C$). Inset of figure 3(c) shows the part of field distribution originating from the vortex state. (d) Temperature dependence of the depolarization rate $\sigma_{sc}(T)$ where the solid line and dotted line are fits to the data employing an isotropic *s*-wave model and a *d*-wave model with line nodes, respectively, using equation (2). Inset of (d) shows the variation of the internal field with temperature.

TF-$\mu$SR studies do not show any signs of the lower transition and additional studies are needed in order to identify the origin of the second transition. There is no difference between the ZF-$\mu$SR data at 0.09 and 4 K, and this supports the view that the second transition is not due to a magnetic impurity. In the presence of a 60 kOe field, the heat capacity jump is fully suppressed. The electronic and lattice heat capacity coefficients, $\gamma$ and $\beta$, respectively, were calculated from the 60 kOe data, which is much higher than the upper critical field, by fitting $C_P(T)/T = \gamma + \beta T^2$, giving a Sommerfeld constant $\gamma = 15.3(1)$ mJ mol$^{-1}$ K$^{-2}$, $\beta = 0.56(1)$ mJ mol$^{-1}$ K$^{-4}$. Using this value of $\beta$ ($= nN_A \frac{12}{5}\pi^4 R\Theta_D^{-3}$, where $R = 8.314$ J mol$^{-1}$ K$^{-1}$, gives a Debye temperature $\Theta_D = 430(4)$ K. The estimated value of $\gamma$ for $LaIr_3$ is very similar to that observed in $CaIr_2$ superconductor [19] and other Ir-based superconductors [17]. In the case of $LaIr_3$, the low value of the Sommerfeld constant may be due to the lack of *f*-orbitals near the Fermi surface. Using the value of heat capacity jump at 2.5 K, the dimensionless parameter $\Delta C_P/\gamma T_C \sim 1$ which is lower than the 1.43 expected in the BCS weak-coupling limit.

### 3.4. Superconducting gap structures

Figures 3(a) and (b) present the time dependence of the TF-$\mu$SR asymmetry spectra around $T_C$ while figure 3(c) shows the corresponding maximum entropy plots. The maximum-entropy (ME) method used to analyze the TF-$\mu$SR data is based on the Burg algorithm [28, 29], which draws on auto-regression prediction techniques. In contrast to Fourier transforms (FT), ME is useful for data collected over short-time windows and for noisy data, and does not suffer from truncation consequences, such as sine wiggle. It provides a simultaneous interpretation of the asymmetry spectra from various detectors with distinct phases to produce a single frequency spectrum. At $T \geqslant T_C$, the muon depolarization is due to static nuclear moments and the resulting field distribution is centred near the applied field $H$. At $T \leqslant T_C$, the muon depolarization has reasonable damping and the field distribution has two components, the first one close to the applied field $H$ and the second shifted to a lower field value. The inset of figure 3(c) shows the portion of the field distribution arising from the vortex lattice. In order to investigate the superconducting order parameters and the pairing mechanism of $LaIr_3$ compound, we have carefully examined the TF-$\mu$SR data. Below $T_C$, the TF asymmetry spectra which decay due to the superconducting vortex state, could be fit by an oscillatory decaying function [31–35],

$$G_{z1}(t) = A_1\cos(\omega_1 t + \Phi)\exp\left(\frac{-\sigma^2 t^2}{2}\right) + A_2\cos(\omega_2 t + \Phi), \quad (1)$$

where $A_1$ and $A_2$ are the transverse field asymmetries, and $\omega_1$ and $\omega_2$ are the frequencies that emerge from the $LaIr_3$ sample and background silver holder respectively. $\Phi$ is the initial phase and $\sigma$ is the total depolarization rate. The superconducting contribution $\sigma_{sc}$ is calculated from $\sigma_{sc} = \sqrt{\sigma^2 - \sigma_n^2}$, where $\sigma_n$ is the nuclear contribution which was obtained from the value of $\sigma$ above $T_C$. The fitting to the lowest temperature TF data yields $A_1 \sim 25\%$ and $A_2 \sim 75\%$. In the TF-$\mu$SR fits shown in figure 3(d), $A_2$ is fixed and $A_1$ is allowed to vary. The inset of figure 3(d) exhibits the onset of superconductivity below $T_C$, which is marked by a drop in the internal field. The temperature dependence of the magnetic penetration depth can be modelled using [30, 31, 34]

$$\frac{\sigma_{sc}(T)}{\sigma_{sc}(0)} = \frac{\lambda^{-2}(T,\Delta_0)}{\lambda^{-2}(0,\Delta_0)} = 1 + \frac{1}{\pi}\int_0^{2\pi}\int_{\Delta(T)}^{\infty}(\frac{\delta f}{\delta E}) \times \frac{E\mathrm{d}E\mathrm{d}\phi}{\sqrt{E^2 - \Delta(T,\Delta)^2}}, \quad (2)$$

where $f = [1 + \exp(-E/k_B T)]^{-1}$ is the Fermi function, $\phi$ is the angle along the Fermi surface, and $\Delta(T,0) = \Delta_0\delta(T/T)g(\phi)$. The superconducting gap was approximated using $\delta(T/T_C) = \tanh[1.82(T_C/T - 1)]^{0.51}$ where $g(\phi)$ gives the angular dependence of gap and $\phi$ is the polar angle for the anisotropy. $g(\phi)$ is replaced with (a) 1 for an isotropic *s*-wave gap and (b) $|\cos(2\phi)|$ for a nodal *d*-wave gap

[36, 37]. For $LaIr_3$, the $\lambda^{-2}(T)$ data can be modelled satisfactorily by employing an isotropic *s*-wave gap with a value of 0.35(1) meV. The gap to $T_C$ ratio is found to be $2\Delta(0)/k_BT_C = 3.31(1)$, which lower than the value 3.56 expected from BCS theory. This suggests weak-coupling superconductivity in the case of $LaIr_3$, which is in agreement with the heat capacity data. TF-$\mu$SR measurements of $Mg_{10}Ir_{19}B_{16}$ reveal spin-singlet *s*-wave pairing, even though the lack of inversion symmetry and large SO coupling of $Mg_{10}Ir_{19}B_{16}$ should produce a mixed pairing state, likely with a large spin-triplet contribution [38]. TF-$\mu$SR data on $La_7Ir_3$ compound also reveal a gap with an isotropic *s*-wave pairing symmetry [39].

The muon depolarization rate below $T_C$ is linked to the magnetic penetration depth, $\lambda$. In case of a triangular [40–42] lattice $\frac{\sigma_{sc}^2}{\gamma_\mu^2} = \frac{0.003\,71\times\phi_0^2}{\lambda^4}$, where $\phi_0 = 2.07\times10^{-15}$ Tm$^2$, is the flux quantum number and $\gamma_\mu/2\pi = 135.5$ MHz T$^{-1}$, is the muon gyromagnetic ratio. From the *s*-wave fit, we estimate that the magnetic penetration depth $\lambda(0) = 386(3)$ nm $\lambda_L(0) = 386(3)$ nm. London's theory [40] gives the relation between $\lambda$ $(= \lambda_L)$ and other microscopic parameters such as $\lambda_L^2 = \frac{m^*c^2}{4\pi n_s e^2}$, where $m^* = (1+\lambda_{e-ph})m_e$ is the effective mass and $n_s$ is the density of superconducting carriers, and hence one can calculate $m^*$ and $n_s$. The electron–phonon coupling constant $\lambda_{e-ph}$ can be calculated using the Debye temperature, $\Theta_D$, and $T_C$ using McMillan's relation, which is also valid in the weak-coupling limit [43, 44].

$$\lambda_{e-ph} = \frac{1.04+\mu^*\ln(\Theta_D/1.45T_C)}{(1-0.62\mu^*)\ln(\Theta_D/1.45T_C)-1.04}, \qquad (3)$$

where $\mu^*$ is the Coulomb pseudo-potential. McMillan states [43] that $\mu^* = 0.1$ is confirmed for the nearly-free electrons metals such as zinc, and $\mu^* = 0.15$ is reasonable for most of the intermetallic superconductors [44–47]. Furthermore, Allen [44] has stated that for conventional metals $\mu^* \leqslant 0.2$. Using $\mu^* = 0.15$ [22], we find $\lambda_{e-ph} = 0.53$. Using the estimated value of $\lambda_{e-ph}$ and $\lambda_L(0)$, the superconducting carrier density is estimated to be $n_s = 2.9(1)\times10^{27}$ carriers m$^{-3}$ and the effective-mass enhancement $m^* = 1.53m_e$ for $LaIr_3$.

### 3.5. Zero-field muon spin relaxation

Figure 4(a) shows the time dependence of ZF asymmetry spectra for $LaIr_3$ at $T \geqslant T_C$ and $T \leqslant T_C$. At $T \leqslant T_C$, there is no change of muon asymmetry spectra compared to the spectra collected at $T \geqslant T_C$, which suggests that time-reversal symmetry is preserved in $LaIr_3$. The ZF data for $LaIr_3$ can be modelled using the damped Kubo–Toyabe (KT) function [34, 48, 49, 50],

$$G_{z2}(t) = A_0 G_{KT}(t)e^{-\lambda t} + A_{bg}, \qquad (4)$$

where

$$G_{KT}(t) = \left[\frac{1}{3}+\frac{2}{3}(1-\sigma_{KT}^2t^2)e^{\frac{-\sigma_{KT}^2t^2}{2}}\right] \qquad (5)$$

the KT function models the change in asymmetry arising from static nuclear moments and $\lambda$, $A_0$, and $A_{bg}$ are the electronic

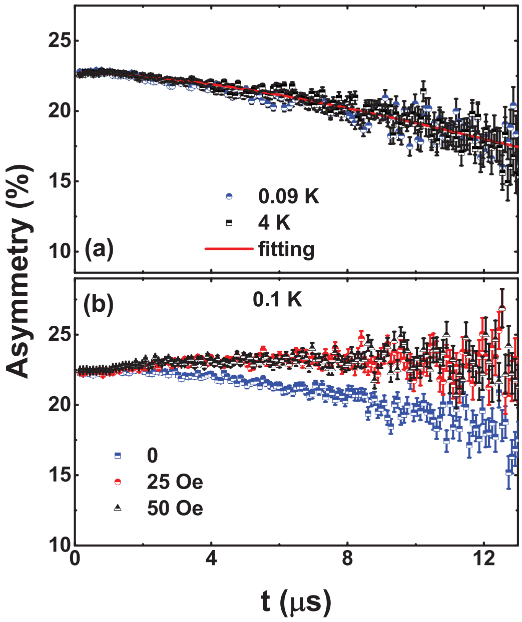


**Figure 4.** (a) Time dependence of ZF asymmetry spectra for $LaIr_3$ collected at 0.09 K (circles) and 4.0 K (squares). The lines are least squares fits to the ZF data made using equations (4) and (5). (b) Longitudinal field asymmetry spectra were taken at 0.1 K in the presence of various applied fields *H*.

relaxation rate, initial sample asymmetry, and background asymmetry, respectively. The fits to the ZF data using equations (4) and (5) give $\sigma_{KT} = 0.041(5)$ $\mu$s$^{-1}$ and $\lambda = 0.018(3)$ $\mu$s$^{-1}$ at 0.09 K and $\sigma_{KT} = 0.041(1)$ $\mu$s$^{-1}$ and $\lambda = 0.013(2)$ $\mu$s$^{-1}$ at 4 K, while the fit parameters $A_0$ and $A_{bg}$ are found to be temperature independent. Furthermore, the ZF-$\mu$SR spectra measured in longitudinal fields of 25 and 50 Oe at 0.1 K (figure 4(b)) revealed the decoupling of the muon spins from the static nuclear fields at the muon stopping sites.

Our ZF-$\mu$SR measurements indicate time-reversal symmetry is preserved in $LaIr_3$. A similar result is found in the Ir-based superconductor $Mg_{10}Ir_{19}B_{16}$ [38], while in the case of $La_7Ir_3$, ZF-$\mu$SR data confirm that the superconducting ground state breaks time-reversal symmetry [39].

## 4. Summary

In summary, we have examined the superconducting gap structure and pairing symmetry of $LaIr_3$ using TF and ZF-$\mu$SR measurements. Bulk type-II superconductivity is observed in the susceptibility measurements with $T_C = 2.5(1)$ K. Similar to $UPt_3$, two transitions are seen in the heat capacity data and the origin of the lower temperature feature remains unclear at this time. Transverse field-$\mu$SR measurements reveal a fully gapped *s*-wave type superconductivity with the gap to $T_C$ ratio, $2\Delta(0)/k_BT_C = 3.31$, compared to 3.56 (BCS value) suggesting weak-coupling superconductivity. Our ZF-$\mu$SR data do not reveal any sign of internal fields below $T_C$, which indicates that time reversal symmetry is preserved in $LaIr_3$. The results underline the need for further research into the properties of Ir-based intermetallic superconductors and especially those that have a noncentrosymmetric structure, where strong antisymmetric SO coupling could lead to unconventional superconductivity, perhaps with a mixed spin singlet-triplet pairing.

## Acknowledgments

AB would like to acknowledge DST India, for an Inspire Faculty Research Grant (DST/INSPIRE/04/2015/000169). DTA and ADH would like to thank CMPC-STFC, Grant No. CMPC-09108, and also DIST for financial support. DTA thanks the Japan Society for the Promotion of Science (JSPS) for an Invitational Fellowship.

## ORCID iDs

A Bhattacharyya https://orcid.org/0000-0002-8037-0487
D T Adroja https://orcid.org/0000-0003-2280-079X
P K Biswas https://orcid.org/0000-0002-7367-5960
M R Lees https://orcid.org/0000-0002-2270-2295
A D Hillier https://orcid.org/0000-0002-2391-8581

## References

[1] Kim B J *et al* 2008 Novel $J_{eff} = 1/2$ Mott state induced by relativistic spin–orbit coupling in $Sr_2IrO_4$ *Phys. Rev. Lett.* **101** 076402
[2] Kim B J, Ohsumi H, Komesu T, Sakai S, Morita T, Takagi H and Arima T 2009 Phase-sensitive observation of a spin–orbital Mott state in $Sr_2IrO_4$ *Science* **323** 1329
[3] Moon S J *et al* 2008 Dimensionality-controlled insulator–metal transition and correlated metallic state in 5*d* transition metal oxides $Sr_{n+1}Ir_nO_{3n+1}$ ($n = 1, 2$, and $\infty$) *Phys. Rev. Lett.* **101** 226402
[4] Hirai D, Takayama T, Hashizume D, Higashinaka R, Yamamoto A, Hiroko A K and Takagi H 2010 Superconductivity in 4*d* and 5*d* transition metal layered pnictides $BaRh_2P_2$, $BaIr_2P_2$ and $SrIr_2As_2$ *Physica* C **470** S296
[5] Kim J *et al* 2012 Magnetic excitation spectra of $Sr_2IrO_4$ probed by resonant inelastic x-ray scattering: establishing links to cuprate superconductors *Phys. Rev. Lett.* **108** 177003
[6] Jackeli G and Khaliullin G 2009 Mott insulators in the strong spin–orbit coupling limit: from Heisenberg to a quantum compass and Kitaev models *Phys. Rev. Lett.* **102** 017205
[7] Singh Y, Manni S, Reuther J, Berlijn T, Thomale R, Ku W, Trebst S and Gegenwart P 2012 Relevance of the Heisenberg–Kitaev model for the honeycomb lattice iridates $A_2IrO_3$ *Phys. Rev. Lett.* **108** 127203
[8] Choi S K *et al* 2012 Spin waves and revised crystal structure of honeycomb iridate $Na_2IrO_3$ *Phys. Rev. Lett.* **108** 127204
[9] Sipos B, Kusmartseva A F, Akrap A, Berger H, Forró L and Tutiš E 2008 From Mott state to superconductivity in 1T-$TaS_2$ *Nat. Mater.* **7** 960
[10] Bauer E, Hilscher G, Michor H, Paul Ch, Scheidt E W, Gribanov A, Seropegin Yu, Noël H, Sigrist M and Rogl P 2004 Heavy fermion superconductivity and magnetic order in noncentrosymmetric $CePt_3Si$ *Phys. Rev. Lett.* **92** 027003
[11] Hanawa N, Muraoka Y, Tayama T, Sakakibara T, Yamaura J and Hiroi Z 2001 Superconductivity at 1 K in $Cd_2Re_2O_7$ *Phys. Rev. Lett.* **87** 187001
[12] Yonezawa S, Muraoka Y, Matsushita Y and Hiroi Z 2004 Superconductivity in a pyrochlore-related oxide $KOs_2O_6$ *J. Phys.: Condens. Matter* **16** L9–12
[13] Guo J G, Qi Y, Matsuishi S and Hosono H 2012 $T_c$ maximum in solid solution of Pyrite $IrSe_2RhSe_2$ induced by destabilization of anion dimers *J. Am. Chem. Soc.* **134** 20001
[14] Suzuki H, Furubayashi T, Cao G H, Kitazawa H, Kamimura A, Hirata K and Matsumoto T 1999 Metal–insulator transition and superconductivity in spinel-type system $Cu_{1-x}Zn_xIr_2S_4$ *J. Phys. Soc. Japan* **68** 2495
[15] Sugitani I *et al* 2006 Pressure-induced heavy-fermion superconductivity in antiferromagnet $CeIrSi_3$ without inversion symmetry *J. Phys. Soc. Japan* **75** 043703
[16] Okamoto Y, Inohara T, Yamakawa Y, Yamakage A and Takenaka K 2016 Superconductivity in the hexagonal ternary phosphide ScIrP *J. Phys. Soc. Japan* **85** 013704
[17] Qi Y P, Guo J, Lei H, Xiao Z, Kamiya T and Hosono H 2014 Superconductivity in noncentrosymmetric ternary equiatomic pnictides La*MP* (***M*** =Ir and Rh; P = P and As) *Phys. Rev.* B **89** 024517
[18] Berry N, Capan C, Seyfarth G, Bianchi A D, Ziller J and Fisk Z 2009 Superconductivity without Fe or Ni in the phosphides $BaIr_2P_2$ and $BaRh_2P_2$ *Phys. Rev.* B **79** 180502
[19] Tütüncü H M, Uzunok H Y, Karaca E, Arslan E and Srivastava G P 2017 Effects of spin–orbit coupling on the electron–phonon superconductivity in the cubic Laves-phase compounds $CaIr_2$ and $CaRh_2$ *Phys. Rev.* B **96** 134514
[20] Hirai D, Ali M N and Cava R J 2013 Strong electron–phonon coupling superconductivity induced by a low-lying phonon in IrGe *J. Phys. Soc. Japan* **82** 124701
[21] Klimczuk T, Ronning F, Sidorov V, Cava R J and Thompson J D 2007 Physical properties of the noncentrosymmetric superconductor $Mg_{10}Ir_{19}B_{16}$ *Phys. Rev. Lett.* **99** 257004
[22] Haldolaarachchige N, Schoop L, Khan M A, Huang W, Ji H, Hettiarachchilage K and Young D P 2017 Ir *d*-band derived superconductivity in the lanthanum–iridium system $LaIr_3$ *J. Phys.: Condens. Matter* **29** 475602
[23] Huber J G 1990 Probing *d*-band superconductivity in $XIr_3$ compounds *Physica* **163** 219–23
[24] Sato Y J, Nakamura A, Shimizu Y, Maurya A, Homma Y, Li D, Honda F and Aoki D 2018 Superconducting properties of $CeIr_3$ single crystal *J. Phys. Soc. Japan* **87** 053704
[25] Geballe T H, Matthias B T, Compton V B, Corenzwit E, Hull G W and Longinotti D 1965 *Phys. Rev.* **137** A119
[26] Pratt F L 2000 WIMDA: a muon data analysis program for the Windows PC *Physica* B **289–90** 710
[27] Trappmann T, Löhneysen H v and Taillefer L 1991 Pressure dependence of the superconducting phases in $UPt_3$ *Phys. Rev.* B **43** 13714
[28] Jones J A and Hore P J 1991 The maximum entropy method. Appearance and reality *J. Magn. Reson.* **92** 363–76
Stephenson D S 1988 Linear prediction and maximum entropy methods in NMR spectroscopy *Prog. NMR Spectrosc.* **20** 515
[29] Rainford B D and Daniell G J 1994 $\mu$SR frequency spectra using the maximum entropy method *Hyperfine Interact.* **87** 1129
[30] Bhattacharyya A *et al* 2019 Evidence of a nodal line in the superconducting gap symmetry of noncentrosymmetric $ThCoC_2$ *Phys. Rev. Lett.* **122** 147001
[31] Bhattacharyya A, Adroja D T, Quintanilla J, Hillier A D, Kase N, Strydom A M and Akimitsu J 2015 Broken time-reversal symmetry probed by muon spin relaxation in the caged type superconductor $Lu_5Rh_6Sn_{18}$ *Phys. Rev.* B **91** 060503
[32] Bhattacharyya A, Adroja D T, Kase N, Hillier A D, Akimitsu J and Strydom A M 2015 Unconventional superconductivity in $Y_5Rh_6Sn_{18}$ probed by muon spin relaxation *Sci. Rep.* **5** 12926

[33] Bhattacharyya A, Adroja D T, Kase N, Hillier A D, Strydom A M and Akimitsu J 2018 Unconventional superconductivity in the cage-type compound $Sc_5Rh_6Sn_{18}$ *Phys. Rev.* B **98** 024511
[34] Adroja D T, Bhattacharyya A, Telling M, Feng Y, Smidman M, Pan B, Zhao J, Hillier A D, Pratt F L and Strydom A M 2015 Superconducting ground state of quasi-one-dimensional $K_2Cr_3As_3$ investigated using $\mu$SR measurements *Phys. Rev.* B **92** 134505
[35] Bhattacharyya A, Adroja D T, Smidman M and Anand V K 2018 A brief review on $\mu$SR studies of unconventional Fe- and Cr-based superconductors *Sci. China-Phys. Mech. Astron.* **61** 127402
[36] Annett J F 1990 Symmetry of the order parameter for high-temperature superconductivity *Adv. Phys.* **39** 83
[37] Pang G M, Smidman M, Jiang W B, Bao J K, Weng Z F, Wang Y F, Jiao L, Zhang J L, Cao G H and Yuan H Q 2015 Evidence for nodal superconductivity in quasi-one-dimensional $K_2Cr_3As_3$ *Phys. Rev.* B **91** 220502
[38] Aczel A A, Williams T J, Goko T, Carlo J P, Yu W, Uemura Y J, Klimczuk T, Thompson J D, Cava R J and Luke G M 2010 Muon spin rotation/relaxation measurements of the noncentrosymmetric superconductor $Mg_{10}Ir_{19}B_{16}$ *Phys. Rev.* B **82** 024520
[39] Barker J A T, Singh D, Thamizhavel A, Hillier A D, Lees M R, Balakrishnan G, Paul D M and Singh R P 2015 Unconventional superconductivity in $La_7Ir_3$ revealed by muon spin relaxation: introducing a new family of noncentrosymmetric superconductor that breaks time-reversal symmetry *Phys. Rev. Lett.* **115** 267001
[40] Sonier J E, Brewer J H and Kiefl R F 2000 $\mu$SR studies of the vortex state in type-II superconductors *Rev. Mod. Phys.* **72** 769
[41] Chia E E M, Salamon M B, Sugawara H and Sato H 2004 Probing the superconducting gap symmetry of $PrRu_4Sb_{12}$: a comparison with $PrOs_4Sb_{12}$ *Phys. Rev.* B **69** 180509
[42] Amato A 1997 Heavy-fermion systems studied by $\mu$SR technique *Rev. Mod. Phys.* **69** 1119
[43] McMillan W L 1968 Transition temperature of strong-coupled superconductors *Phys. Rev.* **167** 331
[44] Allen P B 1999 *Handbook of Superconductivity* ed C P Poole (New York: Academic) ch 9 p 478
[45] Verchenko V Y, Tsirlin A A, Zubtsovskiy A O and Shevelkov A V 2016 Strong electron–phonon coupling in the intermetallic superconductor $Mo_8Ga_{41}$ *Phys. Rev.* B **93** 064501
[46] Singh D, Hillier A D, Thamizhavel A and Singh R P 2016 Superconducting properties of the noncentrosymmetric superconductor $Re_6Hf$ *Phys. Rev.* B **94** 054515
[47] Carnicom E M *et al* 2018 $TaRh_2B_2$ and $NbRh_2B_2$: superconductors with a chiral noncentrosymmetric crystal structure *Sci. Adv.* **4** eaar7969
[48] Adroja D T, Bhattacharyya A, Biswas P K, Smidman M, Hillier A D, Mao H, Luo H, Cao G-H, Wang Z and Wang C 2017 Multigap superconductivity in ThAsFeN investigated using $\mu$SR measurements *Phys. Rev.* B **96** 144502
[49] Adroja D T, Bhattacharyya A, Smidman M, Hillier A, Feng Y, Pan B, Zhao J, Lees M R, Strydom A M and Biswas P K 2017 Nodal superconducting gap structure in the quasi-one-dimensional $Cs_2Cr_3As_3$ investigated using $\mu$SR measurements *J. Phys. Soc. Japan* **86** 044710
[50] Bhattacharyya A, Adroja D T, Hillier A D, Jha R, Awana V P S and Strydom A M 2017 Superconducting gap structure in the electron doped $BiS_2$-based superconductor *J. Phys.: Condens. Matter* **29** 265602